Geometric-phase-effect tunnel-splitting oscillations in single-molecule magnets with fourth-order anisotropy induced by orthorhombic distortion

M. S. Foss-Feig[(a)] and Jonathan R. Friedman[(b)]

Department of Physics, Amherst College - Amherst, MA 01002-5000, USA

Abstract – We analyze the interference between tunneling paths that occurs for a spin system with both fourth-order and second-order transverse anisotropy. Using an instanton approach, we find that as the strength of the second-order transverse anisotropy is increased, the tunnel splitting is modulated, with zeros occurring periodically. This effect results from the interference of four tunneling paths connecting easy-axis spin orientations and occurs in the absence of any magnetic field.

Geometric-phase effects play an important role in spin dynamics. Notably, a geometric phase lies at the heart of spin-parity effects, such as Kramers degeneracy [1–3]. Tunneling of a spin (or magnetic particle) between degenerate orientations can be modulated by such geometric-phase effects via the interference between multiple tunneling paths, with complete suppression (or "quenching") of the tunnel splitting occurring when tunneling paths destructively interfere.

Garg has considered the case in which the tunneling of a spin with biaxial anisotropy can be modulated by the application of a magnetic field along the hard axis [4,5]. Specifically, he studied the Hamiltonian

$$\mathcal{H} = D(J^2 - \hat{J}_z^2) + E(\hat{J}_x^2 - \hat{J}_y^2) - h_x\hat{J}_x, \qquad (1)$$

for spin J and anisotropy constants $D > E > 0$ and $h_x \equiv g\mu_B H_x$. He showed periodic quenching of the tunnel splitting as a function of magnetic field H_x due to geometric-phase interference between tunneling paths. Several extensions and variants of this problem have been studied theoretically [5–18]. In a ground-breaking experiment, Wernsdorfer and Sessoli [19] found clear evidence of this effect in the single-molecule magnet Fe_8, which is reasonably well described by eq. (1).

The case originally studied by Garg involved no magnetic field along the longitudinal (z) direction. Tunneling can occur between the metastable ground state $|J\rangle$ and an excited state $|-J+n\rangle$ when the applied field brings them into resonance, *i.e.*, when $h_z \equiv g\mu_B H_z = nD$, $n = 0, 1, 2, \ldots, 2J-1$ [20]. In Fe_8, it was discovered that at these resonance longitudinal fields, a transverse field along the hard axis continued to produce interference effects [19]. Thus, at certain values of h_z and h_x, destructive interference occurs, suppressing tunneling. These so-called diabolical points in h_z-h_x parameter space have been studied theoretically by several authors using different approaches [5–7,10,11,15,17].

The Mn_{12} single-molecule magnet has a fourfold transverse magnetic anisotropy and, like Fe_8, displays resonant tunneling between two easy-axis orientations [20]. One variant of this molecule, Mn_{12}-tBuAc, appears to display the fourfold symmetry with high accuracy [21–23]. Here we consider the interference that occurs between tunneling paths in such a system and how that interference can be modified by the presence of a second-order transverse anisotropy perturbation. Such a perturbation could potentially be induced by the application of uniaxial pressure to a sample of Mn_{12}. We find that the tunnel splitting is periodically quenched as a function of the strength of the perturbation. This interference effect takes place *in the absence of any magnetic field*. In addition, we find a

(a)Present address: *Department of Physics, University of Colorado - Boulder, CO 80309, USA*.
(b)E-mail: jrfriedman@amherst.edu

pattern of diabolical points in parameter space when a longitudinal field h_z is applied.

Several investigations have studied the inclusion of a fourth-order transverse anisotropy as a perturbation in eq. (1) that affects the number and positions of quenches produced by the external field [5,11,16,17,19]. Other work has studied how a transverse magnetic field modulates the interference among the four tunneling paths defined by a fourth-order transverse anisotropy [12,13]. In the present study the fourth-order anisotropy term is the primary transverse anisotropy in the problem, producing four interfering paths, but the interference is modulated by the strength of the second-order anisotropy, leading to periodic quenches as that term is varied. In particular, we consider a spin governed by the Hamiltonian

$$\mathcal{H} = D\left(J^2 - \hat{J}_z^2\right) + k\left(\hat{J}_+^4 + \hat{J}_-^4\right) + \lambda\left(\hat{J}_x^2 - \hat{J}_y^2\right), \quad (2)$$

where the $\hat{J}$'s are standard spin operators. We restrict the values of k and λ such that the z axis is the spin's easy axis (see appendix).

We calculate the ground-state tunnel splitting using an instanton approach, valid in the semi-classical limit of large J. Since we are considering tunneling between energy minima, there can be no classical trajectories connecting the endpoints of the motion. The quantum trajectories with the largest amplitude are the instantons, obtained from the Euclidean (imaginary-time) Lagrangian

$$L_{\mathrm{E}} = L(t \to -i\tau) = iJ\left(\cos\theta - 1\right)\frac{\mathrm{d}\phi}{\mathrm{d}\tau} - \mathcal{H}(\theta, \phi), \quad (3)$$

where $\mathcal{H}(\theta, \phi)$, the Hamiltonian expressed in terms of spherical angles, is identified with the spin's classical energy $E_{\mathrm{cl}}(\theta, \phi)$ defined in eq. (6) below. Since the instanton paths are extrema of the action in imaginary time, the total energy must be a conserved quantity along each path.

The ground-state (zero-temperature) tunneling rate is given by

$$\Delta = \sum_i \gamma_i\, e^{-S_{\mathrm{E},i}}, \quad (4)$$

where the sum is over all instantons and the pre-factors γ_i arise from integrating the fluctuations around the instanton paths [24]. The Euclidean action S_{E} for an instanton path is

$$S_{\mathrm{E}} = -\int_{\tau_i}^{\tau_f} L_{\mathrm{E}}\mathrm{d}\tau$$
$$= iJ\int_{\phi(-\infty)}^{\phi(+\infty)} (1 - \cos\theta)\mathrm{d}\phi + \int_{\tau_i}^{\tau_f} \mathcal{H}(\theta, \phi)\mathrm{d}\tau. \quad (5)$$

The first term has the form of a Berry phase: The difference in the imaginary part of the action between two paths is proportional to the real part of the solid angle (on the complexified unit sphere) circumscribed by the two paths. Since the last term is the total energy, it is a
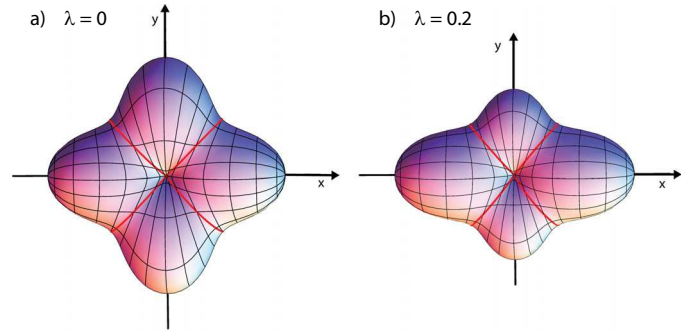

Fig. 1: (Color online) Three-dimensional plot of energy landscape for a spin governed by eq. (6) with $a \equiv kJ^2 = 0.1$ and $\lambda = 0$ (a) or $\lambda = 0.2$ (b). The energy minima are along the z axis (into and out of the page) while the x and y axes are the hard axes. The solid red curves show the four instanton paths with only the real parts of θ and ϕ displayed. These paths were numerically calculated using eqs. (7) and (10). A rather large value of a is used here to ease visual representation. For Mn_{12}, $a \approx 3 \times 10^{-3}$.

constant for an instanton path and, by construction, zero for the Hamiltonian, eq. (2).

For the case of eq. (2), the spin dynamics can be understood in terms of four instanton paths along the complexified unit sphere. When $\lambda = 0$, the spin's energy has four saddle points located in the x-y plane, with instanton paths connecting the $+z$ and $-z$ directions virtually "passing through" these saddle points, as shown in fig. 1(a), where the solid red curves show numerically calculated instanton paths with only the real parts of θ and ϕ being displayed. For $\lambda > 0$, the energy landscape is changed, as shown in fig. 1(b), and the instanton paths are pulled toward the y axis. Reflection symmetry in the x-z and y-z planes requires that all four paths have the same amplitude, but each has a different geometric phase that leads to interference. We therefore concern ourselves with calculating the imaginary part of the action. The interference effect can be understood by considering, say, the top two paths in fig. 1. The solid angle between these paths decreases with increasing λ, modulating the interference between their tunneling amplitudes. An identical effect occurs for the bottom two paths.

For ease of computation we measure energy in units of D (i.e., we set $D = 1$). We choose slightly unconventional spherical coordinates, with the polar angle θ measured from the x axis and the azimuthal angle ϕ measured from the y axis to avoid having coordinate singularities at the poles. In terms of these angles, the classical energy associated with eq. (2) is

$$\begin{aligned} E_{\mathrm{cl}}(\theta, \phi) = {}& J^2(1 - \sin^2\theta\sin^2\phi) \\ & + \lambda J^2(\cos^2\theta - \sin^2\theta\cos^2\phi) \\ & + 2kJ^4(\cos^4\theta + \sin^4\theta\cos^4\phi \\ & - 6\cos^2\theta\sin^2\theta\cos^2\phi), \quad (6) \end{aligned}$$

which has two degenerate absolute minima (with $E_{\mathrm{cl}} = 0$) at $\theta = \pi/2$, $\phi = \pm\pi/2$.
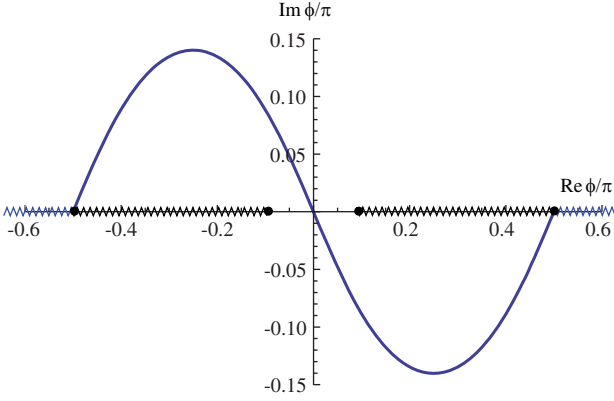
Fig. 2: (Color online) Instanton contour in the complex-ϕ plane for $a = 10^{-4}$ and $\lambda = 0$. Branch points and branch cuts are shown. The contour changes only slightly as a is varied by orders of magnitude.

We can quickly gain a large amount of information about the instantons by solving eq. (6) for the $\theta(\phi)$ paths that conserve energy. Making the substitution $p = J\cos\theta$, the conjugate momentum to ϕ, the instantons must satisfy the constraint $E_{cl} = 0$, which has four solutions:

$$p_{\pm,\pm}(\phi) = \pm J \sqrt{\frac{A(\phi) \pm i\sqrt{B(\phi)}}{C(\phi)}}, \qquad (7)$$

where the subscripts refer to the choices of signs and

$$
\begin{aligned}
A(\phi) &= 4a\cos^4\phi + 12a\cos^2\phi - \sin^2\phi - \lambda\cos^2\phi - \lambda, \\
B(\phi) &= -\left(128a^2 + 16a(\lambda-2) + (\lambda-1)^2\right)\cos^4\phi \\
&\quad + 2\left(1 - \lambda^2 + 8a(\lambda+2)\right)\cos^2\phi - (\lambda+1)^2, \\
C(\phi) &= 4a(\cos^4\phi + 6\cos^2\phi + 1), \qquad (8)
\end{aligned}
$$

with $a \equiv kJ^2$.

Two of the solutions in eq. (7), $p_{\pm,+}$, do not have values of $p = 0$ at the endpoints $\phi = \pm\pi/2$. While such "boundary-jump instantons" [11] are allowed solutions, numerical evaluation of these solutions shows that their action is much larger than for the other two solutions and therefore they give negligible contribution to the tunnel splitting. We neglect them in further discussion.

The other solutions $p_{\pm,-}$ for $0 < a < 1/2$ and $|\lambda| < \lambda_c \equiv 4\sqrt{a - 2a^2}$ have four branch points along the real-ϕ axis at $\phi = \pm\pi/2$ and at the zeros of $B(\phi)$. Evaluating the action along the real-ϕ axis is then potentially problematic and the integration contour must be chosen with some care. A judicious choice of branch cuts is shown in fig. 2. We find the instanton trajectories by considering the (imaginary) time dependence of the coordinates.

The equations of motion for the variables ϕ and p can be found using Hamilton's equations:

$$
\begin{aligned}
\dot{\phi} = -2i\, Jp(4ap^2 + J^2\sin^2\phi + \lambda J^2(1+\cos^2\phi) \\
+ 12a(2p^2 - J^2)\cos^2\phi + 4a(J^2 - p^2)\cos^4\phi)/J^2, \quad (9)
\end{aligned}
$$

Table 1: Instanton actions: the upper bound $-\pi/2$ *vs.* $3\pi/2$ is intended to convey whether the instanton runs through 0 or π.

Instanton	Euclidean action
1	$iJ\int_{\pi/2}^{-\pi/2}(1 - p_{+,-}(\phi))\mathrm{d}\phi$
2	$iJ\int_{\pi/2}^{3\pi/2}(1 - p_{-,-}(\phi))\mathrm{d}\phi$
3	$iJ\int_{\pi/2}^{-\pi/2}(1 - p_{-,-}^*(\phi))\mathrm{d}\phi$
4	$iJ\int_{\pi/2}^{3\pi/2}(1 - p_{+,-}^*(\phi))\mathrm{d}\phi$

$$
\begin{aligned}
\dot{p} = -i\sin(2\phi)(J^2 - p^2)(2a(J^2 - 7p^2) + J^2(1-\lambda) \\
+ 2a(J^2 - p^2)\cos(2\phi))/J^2. \quad (10)
\end{aligned}
$$

Equation (9) can be decoupled by substituting one of the solutions $p_{\pm,-}$ for p. The equation can then be solved numerically to find the real and imaginary parts of $\phi(\tau)$. For each choice of $p_{\pm,-}$, we find two solutions: one with endpoints at $\phi = \pm\pi/2$ (passing through $\phi = 0$) and the other with endpoints $\phi = \pi/2$ and $3\pi/2$ (passing through $\phi = \pi$) (see footnote [1]). Four more solutions can be found by noting that eqs. (9) and (10) are invariant under the transformation $(\phi \to -\phi^*, p \to p^*)$ followed by complex conjugation of the equations. This yields a total of eight solutions, four of which are instantons and four anti-instantons. These can be sorted by using eq. (9) to determine the sign of $\dot{\phi}$ at the midpoint of each solution. Table 1 indicates the Euclidean action integrals for the four instantons, with the limits designating the direction of the path about the polar axis.

By symmetry, only one of these integrals need actually be evaluated. The contour in the complex-ϕ plane associated with one of these solutions (Instanton 1) is shown in fig. 2. That the contour begins and ends at a branch point poses no complications since the integrand vanishes smoothly at those points. With the branch cuts shown, the contour can be continuously deformed onto (or within ε of) the real-ϕ axis. Along this axis, the real part of $p_{\pm,-}$ (the part we are interested in) is only non-zero between the inner two branch points. The imaginary part of the Euclidean action (for Instanton 1) can then be written as

$$
\begin{aligned}
S_I &= -J(\pi + I), \\
I &= \frac{1}{J}\int_b^{-b} \mathrm{Re}\left[p_{+,-}(\phi)\right]\mathrm{d}\phi, \quad (11)
\end{aligned}
$$

where $\pm b$ are the positions of the inner branch points. Proceeding similarly for the other instantons, the total tunnel splitting can be calculated using eq. (4):

$$
\begin{aligned}
\Delta(\lambda) &\propto e^{-S_R}\left[e^{-iJ\pi}\left(e^{-iJI} + e^{iJI}\right)\right. \\
&\quad \left. + e^{iJ\pi}\left(e^{-iJI} + e^{iJI}\right)\right] \\
&= 4e^{-S_R}\cos(J\pi)\cos(JI), \quad (12)
\end{aligned}
$$

---

[1]While our numerical calculations show that each is a solution, we have not proven that these are the *only* solutions. However, we do not expect more than four instanton solutions with equal magnitude actions given the symmetry of the problem.

where S_R is the real part of the Euclidean action and the same for all instantons. The factor $\cos(J\pi)$ ensures that the tunnel splitting is zero for half-integer spin, in accordance with Kramers' theorem [1,2]. It arises from the interference between diametrically opposite paths (fig. 1) that remains constructive (destructive) for integer (half-integer) values of J as λ is varied. The $\cos(JI)$ factor is of chief concern here. Since the integral I depends on anisotropy parameters a and λ, variations in these parameters can modulate the tunnel splitting, with complete suppression of tunneling when $JI = (2n+1)\pi/2$ for integer n. For fixed a, as λ is increased from zero, the inner branch points move towards each other and the value of I decreases, resulting in repeated suppression of tunneling until $\lambda = \lambda_c \equiv 4\sqrt{a - 2a^2}$ at which point $b = 0$ and the value of I goes to zero.

An approximate expression for I can be obtained by treating the integrand as a function of two independent parameters (a and λ/λ_c) and expanding in a power series in a. The resulting integrals can be done by elementary means. We obtain

$$I = \frac{\pi}{2}\left(1 - \frac{\lambda}{\lambda_c}\right) g(a, \lambda),\tag{13}$$

where, up to order a^2,

$$g(a, \lambda) = 1 + \frac{\lambda}{\lambda_c}\left(1 + \frac{\lambda}{\lambda_c}\right)$$
$$\times \left(\frac{3a}{2} - \frac{a^2}{16}\left(9 - 133\left(\frac{\lambda}{\lambda_c}\right)^2\right)\right).\tag{14}$$

Figure 3 compares the results of eqs. (13) and (14) (solid blue curve) to exact numerical evaluation of I (points) for $a = \frac{2-\sqrt{2}}{8} \approx 0.073$, the largest value of a for which I can be meaningfully evaluated for all $\lambda < \lambda_c$ (see appendix). Even at this relatively large value for a, eq. (13) is clearly an excellent approximate expression for I, although for such large values of a and λ the instanton approximation is questionable since the barrier has nearly disappeared. The λ-dependence of I is clearly dominated by the $(1 - \frac{\lambda}{\lambda_c})$ factor in eq. (13), responsible for the nearly linear behavior seen in the figure. To illustrate the geometric interference effect, the figure also shows the behavior of the magnitude of the $\cos(JI)$ factor in Δ as a function of λ (red dashed curve) for $J = 10$. We note that when J is an odd integer, the zeros in Δ start at $\lambda = 0$ (because $I = \pi/2$ at this point), as expected by general symmetry considerations [2]. Since the argument of $\cos(JI)$ ranges from zero to $J\pi/2$, the number of zeros is $\lfloor (J+1)/2 \rfloor$.

We next investigated the effect of a longitudinal field on the geometric-phase interference. Such a field introduces a term $-h_z S_z$ into the Hamiltonian, breaking the symmetry between up and down directions of spin (i.e., raising the energy of one minimum with respect to the other) but preserving other rotational and reflection symmetries. In
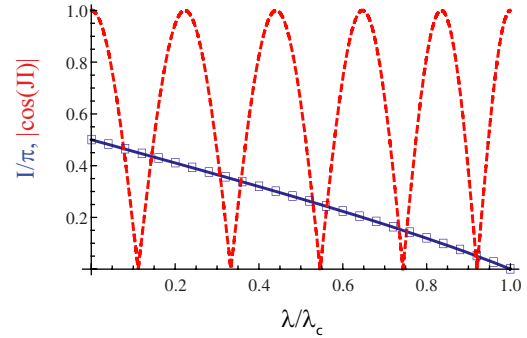

Fig. 3: (Color online) I/π (blue, solid curve and points) and $|\cos(JI)|$ (red, dashed) as a function of λ/λ_c for $a = \frac{2-\sqrt{2}}{8}$ and $J = 10$. The points are the result of numerical evaluation of I whereas the solid blue curve is obtained using eq. (13). The value of a used is the largest one for which the problem is well defined for all values of $\lambda < \lambda_c$ (see appendix).

particular, the four instanton paths maintain the same amplitude and will continue to interfere.

Similar to what was found for the biaxial spin, we determined that a spin described by eq. (2) has an array of diabolical points. At certain values of longitudinal field, varying λ causes the tunnel splitting to oscillate, with perfect degeneracies occurring at a discrete set of points in λ-h_z space. The effect can be most readily addressed by invoking the argument of Bruno [17] that tunneling between $|J\rangle$ and $|-J + n\rangle$ can be mapped approximately onto the problem of tunneling between the ground states $|\tilde{J}\rangle$ and $|-\tilde{J}\rangle$ of an effective spin $\tilde{J} = J - n/2$ in zero magnetic field. Making the substitution $J \to \tilde{J}$ in eqs. (12) and (13) and keeping in mind that both a and λ_c are functions of J, we can generate the full set of diabolical points. If a is small, we can approximate $g(a, \lambda) \approx 1$ and get the following simple expressions for the diabolical points:

$$h_z = nD,$$
$$\lambda = 4\sqrt{kD - 2(k\tilde{J})^2}[\tilde{J} - 2l - 1],\tag{15}$$

where $l = 0, 1, \ldots, \lfloor(\tilde{J} - 1)/2\rfloor$ and n is an even (odd) integer when J is a (half-)integer. For other integer values of n, eq. (12) yields exactly zero tunnel splitting for all values of λ, as expected in the absence of a transverse field. In these expressions, we have restored the anisotropy parameter D. The first expression is equivalent to the condition for resonant tunneling [20] in which the ground state associated with the up direction is resonant with the n-th excited state in the down direction. Figure 4 shows a comparison between the results of eq. (15) and exact numerical diagonalization of the Hamiltonian using $J = 10$ and $k/D = 2 \times 10^{-5}$, a value close to that of Mn_{12}. The agreement is obviously very good.

We note that the pattern of diabolical points in fig. 4 resembles the pattern found in the biaxial system [5–7, 10,11,15,17], where the diabolical points lie on a perfect
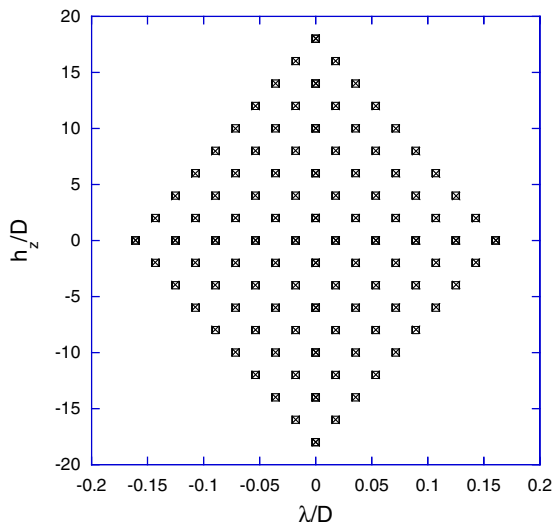
Fig. 4: (Color online) Diabolical points in λ-h_z parameter space with $k = 2 \times 10^{-5}D$ and $J = 10$ (*i.e.*, Mn$_{12}$) calculated using eq. (15) (squares) and by exact diagonalization of the Hamiltonian (×'s). Points at negative values of h_z and λ were obtained by reflection in the horizontal and/or vertical axis.

Fig. 5: (Color online) Parameter-space plot indicating the essential features of the spin's energy landscape. The unshaded region represents the locus of parameters to which the analysis in this paper applies. In the shaded region on the right, the saddle points on the equator have become local minima. In the shaded region above $\lambda = 1$, the minima at the poles have bifurcated. The dashed line indicates where equatorial saddle points merge pairwise. The solid curve shows the behavior of λ_c and is included for reference.

lattice in h_x-h_z space. In contrast, the diabolical points in fig. 4 lie in the λ-h_z plane and only form a perfect lattice in the limit of $k \to 0$.

Finally, we consider the feasibility of observing the proposed effect. For Mn$_{12}$Ac, $a \approx 3 \times 10^{-3}$, which gives $\lambda_c \approx 0.2D = 0.11\,$K. Density functional calculations that include molecules of solvation in a trans configuration estimate that a 3% strain along the axis defined by the solvent molecules can produce changes in λ as large as 19 mK [25]. To the best of our knowledge, the elastic modulus of Mn$_{12}$Ac has not been measured, but it is unlikely that it could be much larger than 100 kbar. One might then need uniaxial pressure as high as 17 kbar to reach λ_c, although the interference effect would manifest at substantially lower values of λ. Several experimental studies have investigated the effect of hydrostatic pressure on Mn$_{12}$ [26–29] and have found significant changes in D with pressures as high as 12 kbar. None of these investigations involved uniaxial pressure, which would be needed to observe the interference effect predicted herein. We note that the ground-state tunnel splitting for Mn$_{12}$Ac is extremely small. However, the splitting increases exponentially for progressively higher levels, suggesting that a pressure-induced effect would be observable in thermally excited states, *i.e.*, by studying the magnetic relaxation in the thermally assisted tunneling regime [20] as a function of pressure. Discussion of the geometric-phase effect in excited levels will be presented elsewhere.

In summary, we predict a geometric-phase interference effect involving four instanton paths that can be modulated by the strength of the second-order transverse anisotropy, leading to a nearly periodic suppression of tunneling in the absence of any external field. In principle,
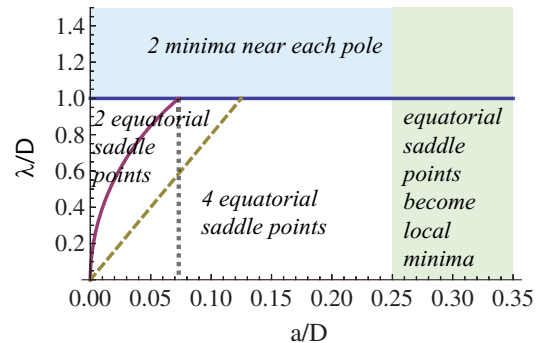
this effect can be experimentally realized through the application of uniaxial stress along one of the hard-axis directions of a fourfold symmetric single-molecule magnet, such as Mn$_{12}$.

$* * *$

Appendix

Here, we discuss how the energy landscape for a spin governed by eq. (6) depends on the anisotropy parameters a and λ. (As in the main text, we measure these anisotropy parameters in units of D and define $a \equiv kJ^2$.) Using standard techniques from multivariable calculus we determined the minima, maxima and saddle points of the landscape.

For small values of a and λ (unshaded region in fig. 5), the landscape resembles that shown in fig. 1 with global minima at the poles ($\pm z$ directions) and saddle points along the equator (x-y plane). As a increases, the saddle points become deeper and for $a > 1/4$ the saddle points transform into local minima on the equator (right shaded region in fig. 5). This limit is far from relevant for Mn$_{12}$, where $a \approx 3 \times 10^{-3}$.

Increasing λ causes pairs of saddle points on the equator to move toward each other (see fig. 1). They merge together when $\lambda = 8a$ (dashed line in fig. 5). Remarkably, even when there are only two saddle points in the potential landscape, there remain four distinct instanton paths. The solid angle between pairs of paths vanishes when $\lambda = \lambda_c$ (solid curve), which does not correspond to any notable

change in the energy landscape. The vertical dashed line represents the values in this parameter space used for the results presented in fig. 3, *i.e.*, a is such that $\lambda_c = 1$.

Finally, when $\lambda > 1$ each energy minimum at a pole bifurcates into two minima, one tilted toward the $+y$ direction and the other toward the $-y$ direction. This substantially changes the nature of the problem. The analysis described in this paper applies only to the unshaded region in fig. 5 and would need modification to handle the energy landscapes corresponding to the shaded regions.

REFERENCES

[1] Loss D., DiVincenzo D. P. and Grinstein G., *Phys. Rev. Lett.*, **69** (1992) 3232.
[2] von Delft J. and Henley C. L., *Phys. Rev. Lett.*, **69** (1992) 3236.
[3] Chudnovsky E. M. and DiVincenzo D. P., *Phys. Rev. B*, **48** (1993) 10548.
[4] Garg A., *Europhys. Lett.*, **22** (1993) 205.
[5] Garg A., in *Exploring the Quantum/Classical Frontier: Recent Advances in Macroscopic Quantum Phenomena*, edited by Friedman J. R. and Han S. (Nova Science, Hauppauge, NY) 2003, p. 219.
[6] Garg A., *Phys. Rev. Lett.*, **83** (1999) 4385; *Europhys. Lett.*, **50** (2000) 382; *Phys. Rev. B*, **64** (2001) 094413; 094414.
[7] Villain J. and Fort A., *Eur. Phys. J. B*, **17** (2000) 69.
[8] Chudnovsky E. M. and Martinez-Hidalgo X., *Europhys. Lett.*, **50** (2000) 395.
[9] Leuenberger M. N. and Loss D., *Phys. Rev. B*, **63** (2001) 054414.
[10] Keçecioğlu E. and Garg A., *Phys. Rev. B*, **63** (2001) 064422.
[11] Keçecioğlu E. and Garg A., *Phys. Rev. Lett.*, **88** (2002) 237205.
[12] Park C. S. and Garg A., *Phys. Rev. B*, **65** (2002) 064411.
[13] Kim G.-H., *J. Appl. Phys.*, **91** (2002) 3289.
[14] Chen Z.-D., *Europhys. Lett.*, **62** (2003) 726.
[15] Kim G.-H. and Kim T.-S., *Phys. Rev. Lett.*, **92** (2004) 137203.
[16] del Barco E., Kent A. D., Hill S., North J. M., Dalal N. S., Rumberger E. M., Hendrickson D. N., Chakov N. and Christou G., *J. Low Temp. Phys.*, **140** (2005) 119.
[17] Bruno P., *Phys. Rev. Lett.*, **96** (2006) 117208.
[18] Leuenberger M. N. and Mucciolo E. R., *Phys. Rev. Lett.*, **97** (2006) 126601.
[19] Wernsdorfer W. and Sessoli R., *Science*, **284** (1999) 133.
[20] Friedman J. R., Sarachik M. P., Tejada J. and Ziolo R., *Phys. Rev. Lett.*, **76** (1996) 3830.
[21] Hill S., Anderson N., Wilson A., Takahashi S., Chakov N. E., Murugesu M., North J. M., Dalal N. S. and Christou G., *J. Appl. Phys.*, **97** (2005) 10M510.
[22] Wernsdorfer W., Murugesu M. and Christou G., *Phys. Rev. Lett.*, **96** (2006) 057208.
[23] Barra A.-L., Caneschi A., Cornia A., Gatteschi D., Gorini L., Heiniger L.-P., Sessoli R. and Sorace L., *J. Am. Chem. Soc.*, **129** (2007) 10754.
[24] Rajaraman R., *Solitons and Instantons: An Introduction to Solitons and Instantons in Quantum Field Theory* (Elsevier Science, Amsterdam) 1989.
[25] Kyungwha Park, private communication.
[26] Murata Y., Takeda K., Sekine T., Ogata M. and Awaga K., *J. Phys. Soc. Jpn.*, **67** (1998) 3014.
[27] Suzuki Y., Takeda K. and Awaga K., *Phys. Rev. B*, **67** (2003) 132402.
[28] Sieber A., Bircher R., Waldmann O., Carver G., Chaboussant G., Mutka H. and Güdel H.-U., *Angew. Chem., Int. Ed.*, **44** (2005) 4239.
[29] Bircher R., Chaboussant G., Dobe C., Güdel H.-U., Ochsenbein S. T., Sieber A. and Waldmann O., *Adv. Funct. Mater.*, **16** (2006) 209.